Microchimica Acta (2021) 188: 86
https://doi.org/10.1007/s00604-021-04743-y

ORIGINAL PAPER

Construction of an electrochemical sensor with graphene aerogel doped with ZrO_2 nanoparticles and chitosan for the selective detection of luteolin

Xiudan Hou[1] · Wei Wu[1] · Fangyuan Zhao[1] · Wancui Xie[2] · Qingli Yang[1]

Received: 20 November 2020 / Accepted: 3 February 2021 / Published online: 15 February 2021
© The Author(s), under exclusive licence to Springer-Verlag GmbH, AT part of Springer Nature 2021

Abstract

A simple, fast and sensitive method for the detection of luteolin is proposed based on the chitosan/reduced graphene oxide aerogel with dispersed ZrO_2 nanoparticles modified glassy carbon electrode (ZrO_2/CS/rGOA-GCE) as an electrochemical sensor. The ZrO_2/CS/rGOA composite was prepared by one pot synthesis from a mixture of GO, CS and zirconyl chloride octahydrate, and subsequently be freeze-dried. Scanning electron microscope images showed a typical thin, wrinkled and fluctuant morphology of graphene nanosheets and the polymerized CS and ZrO_2 nanoparticles deposited on the surface of rGOA. Cyclic voltammetry and differential pulse voltammetry were used to measure the electrochemical response of ZrO_2/CS/rGOA composite-based biosensor towards luteolin at the working potential window (−0.8–0.8 V). The improved performance of this biosensor was attributed to efficient electron transfer and large surface area of 3D rGOA, and high specific activity of Zr towards adjacent hydroxyl groups. Under optimized conditions, the analytical performance of this method towards luteolin was investigated with a detection limit of 1 nM and a linear range from 5 nM to 1000 nM.. Finally, the ZrO_2/CS/rGOA-GCE electrochemical method coupled with solid phase extraction was used for the detection of luteolin in real samples. Recoveries of spiked samples with different concentrations were in the range 78.6–103.3% with a relative RSD lower than 12.0%.

Keywords Electrochemical sensor · Voltammetric detection · Graphene aerogel · Chitosan · Zirconium nanoparticles · Luteolin

Introduction

Luteolin as an important flavonoid is widely existed in many plants and food, which gains of particular interest for the biochemical and pharmacological activities. It is of importance for the investigation of the redox process and electrocatalytic capability, the precise and sensitive detection of luteolin. Nowadays, various measurement methods have been established for the identification and determination of luteolin, such as spectrophotometry [1], high performance liquid chromatography, gas chromatography [2], capillary electrophoresis [3, 4], mass spectrometry and electrochemical sensing method [5–7]. In the above-mentioned technique, there are more or less drawbacks, i.e., time-consuming, complicated operation, high cost, etc. Relatively, the electrochemical technique is an attractive approach due to its low consumption of time and cost, real-time detection, high sensitivity and accuracy, supernal selectivity and simplicity, and more effective practicability. However, it is still a challenge to construct a superior electrode material with high sensitivity and selectivity for luteolin in analytical applications [6, 8–10].

On the basis of the previous researches, an ideal electrocatalyst should possess remarkable properties like good electrical conductivity, fast mass transfer, high specific surface area and porosity, inherent virtue of active sites, excellent chemical and mechanical stability [11–15]. Graphene, as a representative carbon nanomaterial, has gained great concern in the electrochemical technique owing to its unique physicochemical properties of large surface area, excellent conductivity and mechanical strength, and ease of functionalization. In the past few years, most of electrode materials based on

✉ Qingli Yang
yql@qau.edu.cn

[1] College of Food Science and Engineering, Qingdao Agricultural University, Qingdao Shandong Province 266109, China

[2] College of Marine Science and Biological Engineering, Qingdao University of Science and Technology, Shandong Qingdao 266042, China

graphene composites have utilized the two-dimensional (2D) structure of single-layer graphene [16, 17]. In recent years, 3D graphene with network and porous structures (e.g., aerogel, hydrogel, foam, sponge etc.) have been preferred as the electrode material [18–20], which could overcome the aggregation problem, improve the inner space and enhance the electron mobility for unblocked mass migration. However, the porous structure of 3D graphene would bring the decrease of mechanical stability easily to cause the collapse. Chitosan (CS), as a natural biopolymer, was widely used in the electrode material due to its good biocompatibility and water permeability, high adhesion ability and mechanical strength, and nontoxicity [21]. CS with abundant amino and hydroxyl groups, would exhibit a high adsorption capacity for biomolecules. Besides, it can also improve the stability of the electrode surface, and serve as the matrix for the immobilization of other materials [22–24].

Nanostructured metal oxides were also regarded as a class of ideal electrode materials [25]. Integrating the conductive polymer and metal oxide into a nanocomposite has been demonstrated as a valuable approach to enhance the conductivity and electrocatalytic property of nanomaterials. Zirconium oxide (ZrO_2) possesses excellent properties of large surface area, favorable conductivity, fast electron transfer kinetics, good mechanical, chemical, thermal stability, and low cost, which was applied in various fields [26–29]. Among, ZrO_2 nanoparticles are of particular interests in the electrochemical field, which can enhance the efficiency of electron transfer kinetic between the electroactive center and the electrode surface [30]. Besides, there is a specific chelation interaction between Zr and O-hydroxyl compounds, and thus ZrO_2 could provide preferential adsorption for luteolin.

The main objective of this work was to develop a rapid, convenient and highly selective electrochemical method for the determination of luteolin utilizing the unique properties of 3D GOA, CS and ZrO_2 and their combined advantages. Herein, ZrO_2/CS/rGOA nanocomposite was prepared via the hydrothermal synthesis and freeze drying. Various surface analysis techniques were used to characterize the morphology and composition of the ZrO_2/CS/rGOA composite. The electrochemical and electrocatalytic properties of 3D ZrO_2/CS/rGOA were further investigated by cyclic voltammetry (CV) and differential pulse voltammetry (DPV).

Experimental

Materials and reagents

Quercetin (≥ 98.5%), luteolin (≥ 98%), apigenin (≥ 98%), myricetin (≥ 98%) were all obtained from Aladdin Chemical Reagent Co. (Shanghai, China). The chemical structures of flavonoids were shown in Fig. 1. Graphite powder, potassium ferricyanide ($K_3[Fe(CN)_6]$, AR), potassium ferrocyanide ($K_4[Fe(CN)_6]$ $3H_2O$, AR) and zirconyl chloride octahydrate ($ZrOCl_2$ $8H_2O$, AR) were brought from Shanghai Macklin Biochemical Co. Ltd. (Shanghai, China). Chitosan, Nafion® 117 solution and hydrazine hydrate (80 wt%) were obtained from Sigma-Aldrich (St. Louis, MO, USA). *N,N*-dimethyformamide (DMF, AR) was brought from Tian in Fuyu Fine Chemical Co. (Tianjin, China).

Apparatus

Electrochemical experiments were performed on a CHI760E electrochemical workstation (Chenhua instruments Co., Shanghai, China). The three-electrode system was consisted of an Ag/AgCl reference electrode, a bare GCE (3 mm diameter) or ZrO_2/CS/3D-RGO/GCE as the working electrode, and a platinum wire counter electrode. The solid phase extraction (SPE) procedure was performed on an 8-port model SPE80 vacuum manifold equipped with a peristaltic pump (Jinan, China). The structure and property of electrode materials were successively characterized by a scanning electron microscope (SEM, JSM-6701F, Japan), an IFS120HR Fourier transform infrared (FT-IR) spectrometer (Thermo Fisher Scientific, USA), a thermal gravimetric analyzer (STA449C, Germany), X-ray photoelectron spectrometer (XPS, ESCALAB 250Xi, USA), BET analyzer (ASAP 2010, Micromeritics, USA).

Synthesis of ZrO_2/CS/rGOA nanocomposite

The GO suspension was prepared using the modified Hummers method as described in the previous work [31]. The prepared procedure of ZrO_2/CS/rGOA nanocomposite was described in detail: (a) 30 mL of GO suspension was placed in a beaker; (b) 0.03 g of CS and 0.3 g of $ZrOCl_2$ $8H_2O$ were successively added, and the mixture were stirred at 1000 rpm for 10 min; (c) 1 mL of hydrazine hydrate (80%) was added into the mixture and immediately transferred to the reaction still holding for 12 h at 180 °C; (d) the obtained product was cooled to room temperature, centrifuged at 6000 rpm, rinsed with distilled water, dried at 70 °C, put in the ultra-low temperature refrigerator at −80 °C for 10 min and then transferred into the freeze dryer for 10 h to obtain the final nanocomposite. GO, CS/rGOA, and ZrO_2/rGOA were also synthesized being similar to the above process. All resultant nanocomposites were stored at 4 °C for the following experiment.

Preparation of ZrO_2/CS/rGOA-GCE sensor

A bare GCE was polished on an emery paper added with 1, 0.3, 0.05 μm alumina slurry in turn. Then it was rinsed

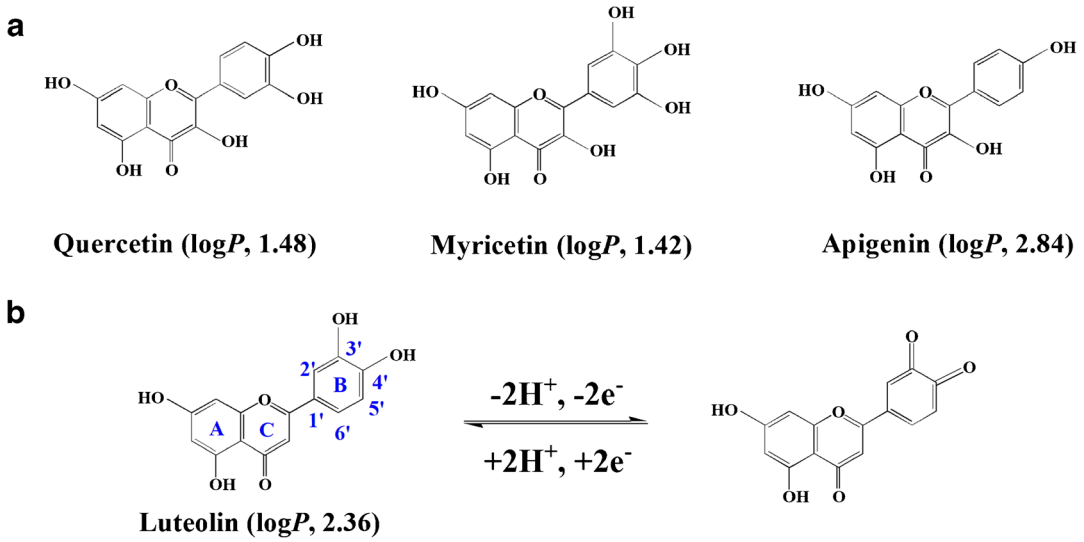

Fig. 1 Chemical structures of different flavonoids and the oxidation mechanism of luteolin

successively with nitric acid (1:1), ethanol and distilled water in an ultrasonic bath for 5 min to remove residual alumina and other impurities. After dried with the nitrogen purging, the peak potential different of the GCE was investigated in the 1 mM $K_3[Fe(CN)_6]/K_4[Fe(CN)_6]$ solution containing 0.1 M KCl until the potential difference reached the standard value. Nafion solution (0.5%, *w*/w) was obtained by diluting the 5% of Nafion solution with DMF. Then, 5 mg of the synthesized 3D ZrO_2/CS/rGOA nanocomposite was added into the 0.5% of Nafion solution and placed into an ultrasonic bath for 2 h to form the uniform black suspension. Next, 3 μL of 3D ZrO_2/CS/rGOA nanocomposite suspension was dropped onto the surface of bare GCE and dried at the room temperature. The preparation process of modified electrode was illustrated in Fig. 2. In the comparative experiment, other prepared electrodes have prepared through the similar procedure.

Sample preparation

The peach juice and red wine were purchased from a local market (Qingdao, China). Firstly, it was filtered with Buchner funnel, and a 12 μm of sieve plate. Then, a solid-phase extraction (SPE) process was performed to remove the impurities. 20 mL of the drink sample was loaded through a SPE vacuum manifold and eluted with 1 mL of methanol. The eluent was evaporated, and dissolved in 100 μL of methanol again.

Electroanalytical measurements

The phosphate buffer solution (0.1 M, pH 6.0) was used as a supporting electrolyte in the determination of luteolin. Before electrochemical measurements, the modified electrolyte was immersed into the flavonoid solution at open-circuit potential for 5 min during the accumulation period. The optimized condition of CV determination was: the working potential window, −0.8 ~ 0.8 V; scanning rate, 100 mV s^{-1}; accumulation time, 5 min; equilibration time, 2 s. The DPV condition was: amplitude of 0.05; pulse width of 0.05 s; pulse period of 0.2 s; equilibration time of 2 s. After each measurement, the modified electrode was immersed into methanol/acetic acid (99:1, *v*/v) stirring for 15 min to remove the residual flavonoid in the last experiment cycle.

Before the measurement of real sample, they were pretreated using the previous method [32]. The detailed procedure was: 30 mL of the sample solution was firstly loaded onto the sorbent of polymeric ionic liquid modified GO grafted silica, and then 0.5 mL of methanol was used to elute the flavonoid. After that, 0.5 mL of eluent was diluted to 30 mL of phosphate buffered solution, which was measured by the ZrO_2/CS/rGOA-GCE.

Results and discussion

Characterization of the modified electrode

The surface morphological feature of electrode materials was investigated. Figure 3 showed SEM images of GOA and ZrO_2/CS/rGOA. The SEM image of GOA exhibited a typical thin, wrinkled and fluctuant morphology of graphene nanosheets. Figure 3 (b, c) showed the polymerized CS and ZrO_2 nanoparticles were deposited on the surface of rGOA, which also brought the decreased surface area. To verify the surface area of electrode materials, the BET adsorption-desorption process was investigated, and results were listed in Table S1.

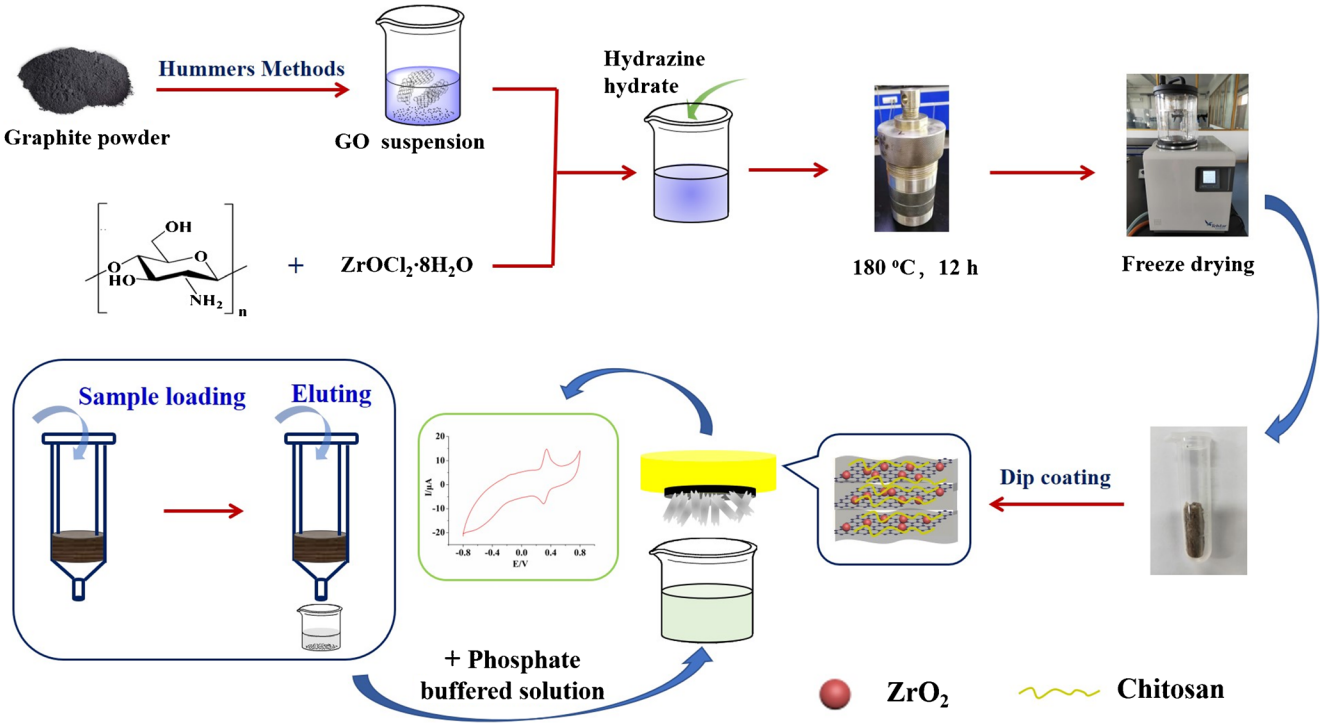

Fig. 2 Preparation schema of the ZrO_2/CS/rGOA modified electrode

The BET surface area, total pore volume and average pore width were 239.16 $m^2\ g^{-1}$, 0.41 $cm^3\ g^{-1}$, 64.43 nm for GOA and 193.86 $m^2\ g^{-1}$, 0.30 $cm^3\ g^{-1}$, 59.66 nm for ZrO_2/CS/rGOA. Due to the introduction of Zr and CS, the surface site of rGOA was occupied, and thus the surface area was slightly decreased.

Figure 4a showed the FT-IR spectra of ZrO_2/rGOA and ZrO_2/CS/rGOA. The broad band at 3382 cm^{-1} was assigned to the stretching vibrations of N-H superimposed on the O-H stretching band, H_2O, and intermolecular hydrogen. The peak observed at 428 cm^{-1} was attributed to the Zr-O vibration. A weak vibration band at 1122 cm^{-1} was related to Zr = O from zirconyl groups, demonstrating that a small amount of $ZrOCl_2$ was complexed by CS/rGOA. The spectrum of ZrO_2/CS/rGOA showed characteristic peaks at 1544 cm^{-1}, 1447 cm^{-1} were assigned to the N-H and C-N band from the CS and -NHCO-.

The XPS analysis was carried out for the rGOA and ZrO_2/CS/rGOA and the spectra were presented in Fig. 4b. As observed the XPS spectra confirm the formation of ZrO_2/CS/rGOA. Compared with GOA, the Zr3d peak was appeared at 183.08 eV in ZrO_2/CS/rGOA. The improvement of C:O content ratio was resulted from the introduction of CS and the reduction of GOA.

The thermal stability of rGOA and ZrO_2/CS/rGOA was studied by TGA. As shown in Fig. 4c, the initial weight loss below 100 °C was mainly ascribed to the evaporation of water molecules presenting in free or bound form in all samples. The weight loss of GOA after 100 °C was attributed to the thermal decomposition of the labile oxygen-containing functional groups and side groups of GOA. The weight loss of ZrO_2/CS/rGOA was mainly due to the decomposition of the polysaccharide ring of CS and slightly oxygen-containing functional groups of rGOA.

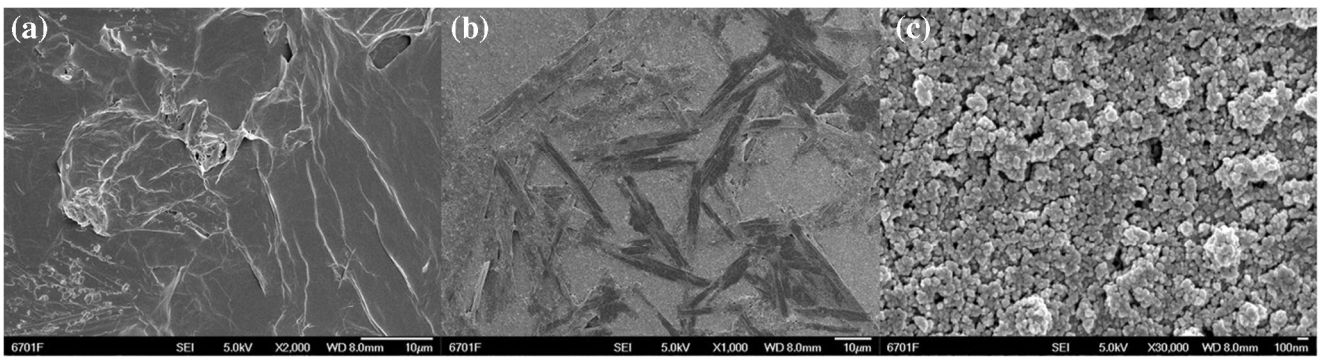

Fig. 3 The surface morphologies of GOA (a) and ZrO_2/CS/rGOA (b, c)

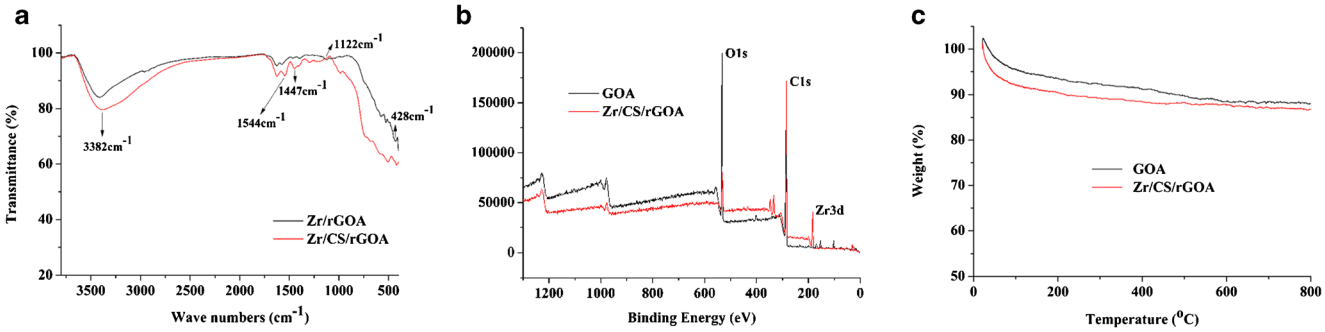

Fig. 4 Characterizations of ZrO_2/CS/rGOA: (a) FT-IR spectra, (b) XPS spectra and (c) TGA analysis

Electrochemical behavior of different modified electrodes

In order to evaluate the electrochemical behavior of bare GCE, CS/rGOA, ZrO_2/rGOA and ZrO_2/CS/rGOA, the CV experiments were performed in 0.1 M pH 6.0 phosphate buffered solution for the detection of luteolin. As shown in Fig. 5(a), there was a pair of small redox peaks appeared at bare GCE. Due to the less conductivity of GO, the GO modified electrode exhibited poor redox peaks. After modified with CS, ZrO_2 and the reduction of GO, it was obviously observed that the current response increased, which was attributed to the adsorption and accumulation of luteolin on the electrode surface. Besides, the reduction of GO would enable the conductivity to be improved. Compared with CS/rGOA, ZrO_2/rGOA possessed lower baseline current. The highest redox peaks occurred at ZrO_2/CS/rGOA-GCE, with a peak-to-peak separation of 0.0399 V. Results indicated that the introduction of both CS, ZrO_2 and rGOA could synergistically improve the adsorption and accumulation of luteolin on the electrode surface and result in the remarkable increase of redox peak current.

Adsorption selectivity and mechanism

A real sample possessed many flavonoids, and due to the similar structure (Fig. 1), others might interfere the determination and analysis of luteolin. Therefore, it was important for investigation of the adsorption selectivity of modified electrode towards luteolin. In this work, the electrochemical behaviors of four flavonoids (quercetin, luteolin, apigenin, myricetin) were investigated by CV and further compared. Figure 5b showed CV curves of the ZrO_2/CS/rGOA-GCE for the determination of luteolin accumulated for 5 min under the open-circuit potential in pH 6.0 phosphate buffered solution including quercetin, myricetin, luteolin, apigenin, respectively. Anodic peaks of luteolin, quercetin and myricetin were 0.344 V, 0.236 V and 0.154 V, respectively. Luteolin possessed obviously higher anodic and cathodic peak currents than other three flavonoids. Apigenin had almost no redox current respond resulted from its weak accumulation on the 3D ZrO_2/CS/rGOA-GCE due to the lack of 3′-hydroxyl group, and the less electrochemical oxidation activity of 4′-hydroxyl electron-donating on B ring and absent 3′-hydroxyl group. It also illustrated the coordination effect between Zr and compound with O-hydroxyl groups. Furthermore, the chelation interaction between Zr and the adjacent hydroxyl group improved the adsorption selectivity of modified electrode towards luteolin due to the easy formation of the five-membered heterocycle.

As shown in Fig. 5c, the as-prepared 3D ZrO_2/CS/rGOA-GCE also exhibited high adsorption selectivity towards luteolin in mixed solution with quercetin, myricetin, luteolin and apigenin. The hydrophilic-hydrophobic property of flavonoids was one of aspects affecting the adsorption selectivity. As shown in Fig. 1, the hydrophobic capacity of luteolin and apigenin were stronger than that of quercetin and myricetin. Therefore, luteolin is more favorable to move to the electrode surface. However, the pH of sample solution had also an effect on the adsorption selectivity of ZrO_2/CS/rGOA-GCE towards analytes. Under the 5 min open-circuit accumulation in pH 4.0 and pH 8.0 phosphate buffered solution containing four flavonoids, there was no selective adsorption of ZrO_2/CS/rGOA-GCE towards luteolin, which also demonstrated the important effect of sample pH on adsorption selectivity. The pH of sample solution not only affected the existing state of flavonoids (ionic or neutral molecules), but also influenced the surface charge and adsorption site of the electrode material. In the coordination process, Zr and the hydroxyl group were the electron donor and electron receptor, respectively. Under the acidic condition, it was difficult to from the coordination interaction between the protonated flavonoids and Zr with the positive charge. Under the basic condition, the excess of free OH^- would be adsorbed on the Zr surface occupying the adsorption site. The adsorption of luteolin onto the surface of ZrO_2/CS/rGOA-GCE could be ascribed to the sufficient adsorption site of ZrO_2/CS/rGOA composite and the adsorption selectivity of Zr towards luteolin.

In addition, some inorganic ions were also selected to evaluate the adsorption selectivity of ZrO_2/CS/rGOA-GCE. In a

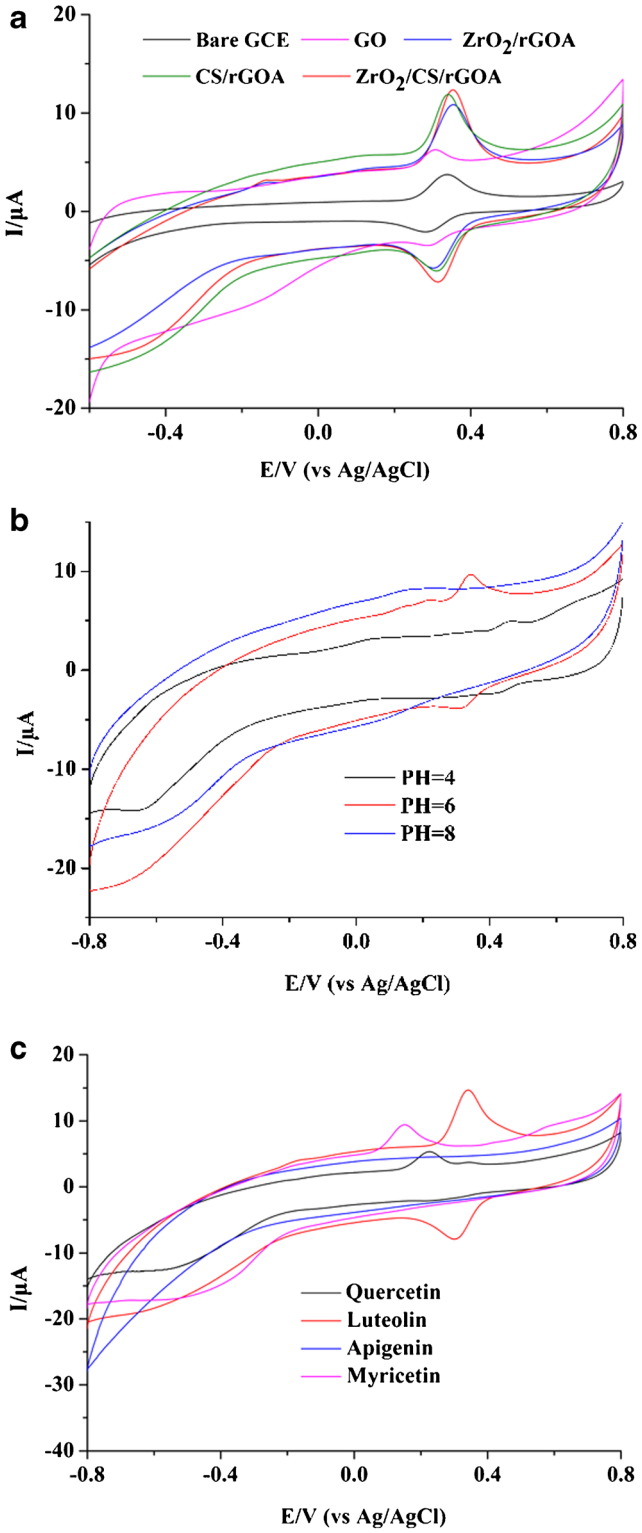

Fig. 5 CVs of different modified electrodes in 0.1 M pH 6.0 phosphate buffered solution containing 2 μM LUT (a), CV curves of ZrO_2/CS/rGOA electrode in pH 6.0 phosphate buffered solution containing different flavonoids (5 μM) (b), and in the mixture solution with different pH containing 5 μM quercetin, 5 μM apigenin, 5 μM myricetin, 1 μM luteolin (c)

mixture of 1 μM luteolin with 100 μM inorganic ions (Na^+, K^+, Mg^{2+}, NH_4^+, Cl^-, SO_4^{2-} etc.), CVs of ZrO_2/CS/rGOA-GCE had no obvious difference suggesting that the selectivity of modified electrode for luteolin was excellent under the open-circuit accumulation process.

Effect of experimental conditions

Accumulation time

The adsorption of analytes on the surface of electrode is a dynamic equilibrium process taking some time to attain a balance. So, the effect of accumulation time on anodic and cathodic peak currents was investigated. As shown in Fig. 6a, peak currents increased rapidly with the accumulation time from 1 to 5 min, and then tended to be balance or even slightly decreased, which resulted from the saturated adsorption of luteolin on the surface of 3D ZrO_2/CS/rGOA-GCE. In the terms of the short analysis time and sensitivity, 5 min of accumulation time was chosen in the following experiments.

Scanning rate

CVs of ZrO_2/CS/rGOA-GCE for the determination of luteolin at different scan rates (20–300 mV s^{-1}) were explored (Fig. 6b), which was obtained in phosphate buffered solution (pH 6.0) s containing 5 μM of luteolin. With the increase of scanning rate, anodic and catholic peak currents would obviously increase, and potential difference was also slightly increase. Therefore, 120 mV s^{-1} was selected as the suitable scanning rate.

The linear relationship of peak current and scanning rate was favorable in the range of 20–300 mV s^{-1}, which could be expressed by the following equation: $I_{pa}(\mu A) = 0.0668\ V(mV\ s^{-1}) + 1.6650$ ($R^2 = 0.9905$), $I_{pc}(\mu A) = -0.0432\ V(mV\ s^{-1})$-0.1271 ($R^2 = 0.9920$). It indicated that the redox reaction of luteolin on the surface of ZrO_2/CS/rGOA-GCE was a reversible and surface-confined process. Results suggested that ZrO_2/CS/rGOA-GCE provided fast electron transfer between the redox center of luteolin and the surface of ZrO_2/CS/rGOA composite. Besides, the redox potential difference of luteolin was almost no shift with the change of scanning rate. and their values were close to 32 mV. And according to Laviron's equation,

$$E_{pa} = E^{0'} + \frac{2.303RT}{(1-\alpha)nF} logv$$

$$E_{pc} = E^{0'} - \frac{2.303RT}{\alpha nF} logv$$

it presented that the electrochemical reaction of luteolin on ZrO_2/CS/rGOA-GCE was a reversible process with two-protons and two-electrodes. The oxidation mechanism of luteolin was shown in Fig. 1b.

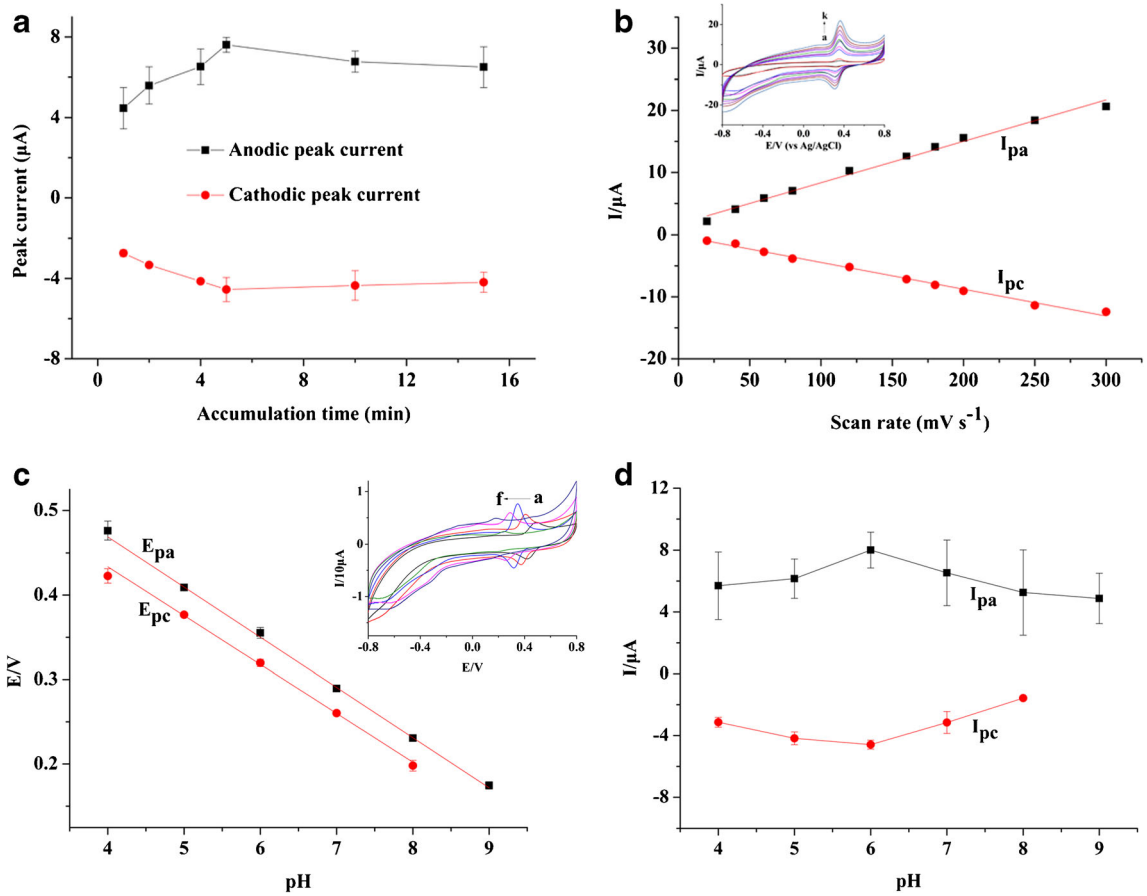

Fig. 6 Effect of the accumulation time at open-circuit potential on anodic and catholic peak currents (a), the linear relationship of I_{pa} and I_{pc} with scanning rates (b), and E_{pa}, E_{pc}, I_{pa} and I_{pc} with pH (c, d), and their CVs of 3D ZrO_2/CS/rGOA/GCE in presence of 5 μM luteolin in phosphate buffered solutions with different pH ranging from 4 to 9 (a → f) and scan rates ranging from 20 to 300 mV s^{-1} (a → k)

pH

The effect of buffer pH on electrochemical responses of luteolin on ZrO_2/CS/rGOA-GCE was explored from pH 4.0 to pH 9.0. Figure 6(c, d) illustrated the influence of pH on peak currents and peak potentials. With the increase of pH, anodic and catholic peak currents would gradually improve and then decrease. They reached the maximum value at pH 6.0, and thus pH 6.0 was selected as the optimized solution pH. Meanwhile, with pH rising, anodic and catholic potentials would shift negatively implying that protons participated in the electrode reaction. In the range of pH 4.0–9.0, there were excellent linear relationship between peak potentials and pH, and the linear equations were as following: $E_{pa}(V) = 0.7068–0.0595pH$ ($R^2 = 0.9994$), $E_{pc}(V) = 0.6651–0.0579pH$ ($R^2 = 0.9977$). It demonstrated that the transfer number of proton and electron were equal in the electrochemical process.

DPV determination of luteolin

DPV responses of luteolin with different concentrations at the ZrO_2/CS/rGOA-GCE sensor were further evaluated under the optimized conditions. Figure 7 showed typical DPVs for luteolin in different concentrations. The sharp and well-defined anodic peak currents at around 0.344 V would rise

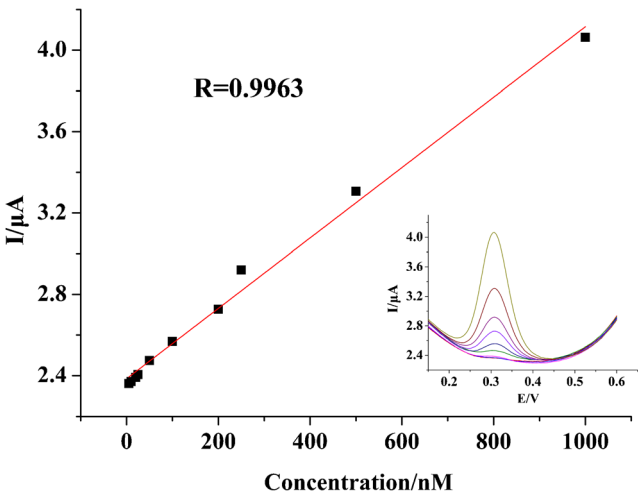

Fig. 7 DPV curves of the ZrO_2/CS/rGOA/GCE with 5 min open-circuit accumulation in 0.1 M pH 6.0 phosphate buffered solution with 5–1000 nM luteolin

linearly with the increased concentration of luteolin in the range from 5 to 1000 nM. The linear regression equation was represented as I(μA) = 0.00173c(nM) +2.385 with a correlation coefficient of 0.9963, and the limit of detection (LOD) was 1 nM at a signal to noise ratio of 3. The result was attributed to desirable active sites of ZrO_2/CS/rGOA and the adsorption of luteolin as well as the electro-catalytic effect at the surface of modified electrode. A comparison of the analytical performance between the proposed ZrO_2/CS/rGOA-GCE and other previous literature sensors for the detection of luteolin was given in Table S1 [6, 33–36]. It could be seen that compared with most reported electrochemical sensors, the as-established 3D ZrO_2/CS/rGOA-GCE sensor presented a wider linear range. However, the limit of detection was not the least, maybe due to the relative higher background baseline of graphene oxide.

Stability and repeatability, reproducibility

The stability and repeatability, reproducibility of ZrO_2/CS/rGOA-GCE electrochemical sensor were investigated, respectively. The as-prepared ZrO_2/CS/rGOA-GCE had been investigated for 40 times, and some detected CV curves were displayed in Fig. S1. With the increase of used times, the peak current and potential were all moved. In the experimental, this prepared electrode had been used for 15 times at one day, and not used in the second day. Single-electrode repeatability was investigated by five replicate detection process of luteolin, and the relative standard deviation (RSD) was 1.2%. Electrode-to-electrode repeatability was evaluated under the same conditions, and RSD obtained from five different electrodes was 8.5%.

Real sample analysis

Peach juice and red wine were detected to test the feasibility of the fabricated ZrO_2/CS/rGOA-GCE sensor. It was found that there was no luteolin in peach juice and red wine. After that, the standard solution of luteolin was spiked into the peach juice and red wine. As shown in Table 1, the obtained recoveries spiked with different standard solutions from two samples ranged from 78.6% to 103.3% with a relative RSD lower than 12.0%. The matrix effect (ME) was also evaluated by an equation: ME (%) = B/A*100, where A was the slope of the calibration curve in the standard solution and B was the slope of the calibration curve of luteolin in real samples, where the calibration curve was obtained through the deduction of background current. Through the calculation, ME values of luteolin in peach juice and red wine were 104.6% and 96.5%, respectively. The results demonstrated that the ZrO_2/CS/rGOA-GCE sensor had a great potential for practice in real samples.

Table 1 Determination of luteolin in samples and the recovery result using the calibration curve method

Sample	Added (nM)	Found (nM)	Recovery (%)	RSD (%)
Peach juice	0	0	–	–
	10	8.1±1.2	81.0	11.6
	50	49.9±2.7	99.8	4.8
	200	206.6±27.0	103.3	11.7
Red wine	0	0	–	–
	10	7.9±1.4	79.0	12.0
	50	39.3±3.9	78.6	5.0
	200	189.0±5.2	94.5	2.5

Conclusion

The ZrO_2/CS/rGOA composite was prepared via a simple hydrothermal synthesis and freeze drying, which was dipping onto the surface of GCE aiming to develop an electrochemical sensor for the detection of luteolin. It was systematically characterized SEM, XPS, FT-IR, and TGA, which also conversely verified the successful synthesis of ZrO_2/CS/rGOA. Through the comparison of different electrodes, it found that the superior electrochemical sensing performance could be directly attributed to the 3D rGOA and the incorporation of ZrO_2 nanoparticles, which not only possessed high surface area but also exhibited specific selective adsorption site and synergistic effects. Coupled to the SPE procedure, the proposed method demonstrated that the LOD of 1 nM for luteolin was not lower than some reported work, but the linear range of 5–1000 nM was relatively wider. The ZrO_2/CS/rGOA electrode exhibited better adsorption selectivity for luteolin than other flavonoids (luteolin, apigenin, myricetin). Finally, this method was also applied for the determination of luteolin in peach juice and red wine samples presenting good recoveries and interference ability. Thus, this as-fabricated sensor was a promising alternative to the traditional analyses for the luteolin detection and could be further exploited for sensing applications.

Supplementary Information The online version contains supplementary material available at https://doi.org/10.1007/s00604-021-04743-y.

Acknowledgments This work was supported by the National Natural Science Foundation of China (No. 31901766, 81703228), Financial support from the Talents of High Level Scientific Research Foundation, Qingdao Agricultural University (No.1119014, 1120023), and Breeding Plan of Shandong Provincial Qingchuang Research Team (2019).

Compliance with ethical standards

Conflict of interest The authors declare that they have no competing of interests.

References

1. Rygula A, Wrobel TP, Szklarzewicz J, Baranska M (2013) Raman and UV–vis spectroscopy studies on luteolin–Al(III) complexes. Vib Spectrosc 64:21–26
2. Bajoub A, Pacchiarotta T, Hurtado-Fernández E, Olmo-García L, García-Villalba R, Fernández-Gutiérrez A, Mayboroda OA, Carrasco-Pancorbo A (2016) Comparing two metabolic profiling approaches (liquid chromatography and gas chromatography coupled to mass spectrometry) for extra-virgin olive oil phenolic compounds analysis a botanical classification perspective. J Chromatogr A 1428:267–279
3. Wu T, Yu C, Li R, Li J (2018) Minireview: recent advances in the determination of flavonoids by capillary electrophoresis. Instrum Sci Technol 46:364–386
4. Xu JJ, An M, Yang R, Cao J, Ye LH, Peng LQ (2016) Trace amounts of poly-beta-cyclodextrin wrapped carbon nanotubes for the microextraction of flavonoids in honey samples by capillary electrophoresis with light-emitting diode induced fluorescence detection. Electrophoresis 37:1891–1901
5. Cao M, Yin X, Bo X, Guo L (2018) High-performance electrocatalyst based on metal-organic framework macroporous carbon composite for efficient detection of luteolin. J Electroanal Chem 824:153–160
6. Feng X, Yin X, Bo X, Guo L (2019) An ultrasensitive luteolin sensor based on MOFs derived CuCo coated nitrogen-doped porous carbon polyhedron. Sensor Actuat B-Chem 281:730–738
7. Hayasaka N, Shimizu N, Komoda T, Mohri S, Tsushida T, Eitsuka T, Miyazawa T, Nakagawa K (2018) Absorption and metabolism of luteolin in rats and humans in relation to in vitro anti-inflammatory effects. J Agric Food Chem 66:11320–11329
8. Cai Y, Huang W, Wu K (2020) Morphology-controlled electrochemical sensing of erbium- benzenetricarboxylic acid frameworks for azo dyes and flavonoids. Sensor Actuat B-Chem 304:127370–127378
9. Gao F, Tu X, Ma X, Xie Y, Zou J, Huang X, Qu F, Yu Y, Lu L (2020) NiO@Ni-MOF nanoarrays modified Ti mesh as ultrasensitive electrochemical sensing platform for luteolin detection. Talanta 215:120891
10. Xie Y, Zhang T, Chen Y, Wang Y, Wang L (2020) Fabrication of core-shell magnetic covalent organic frameworks composites and their application for highly sensitive detection of luteolin. Talanta 213:120843
11. Anik U, Timur S, Dursun Z (2019) Metal organic frameworks in electrochemical and optical sensing platforms: a review. Microchim Acta 186:196
12. Asadian E, Ghalkhani M, Shahrokhian S (2019) Electrochemical sensing based on carbon nanoparticles: a review. Sensor Actuat B-Chem 293:183–209
13. Liu X, Long L, Yang W, Chen L, Jia J (2018) Facilely electrodeposited coral-like copper micro−/nano-structure arrays with excellent performance in glucose sensing. Sensor Actuat B-Chem 266: 853–860
14. Vogiazi V, de la Cruz A, Mishra S, Shanov V, Heineman WR, Dionysiou DD (2019) A comprehensive review: development of electrochemical biosensors for detection of cyanotoxins in freshwater. ACS Sens 4:1151–1173
15. Wang Y, Zeng Z, Qiao J, Dong S, Liang Q, Shao S (2021) Ultrasensitive determination of nitrite based on electrochemical platform of AuNPs deposited on PDDA-modified MXene nanosheets. Talanta 221:121605–121612
16. Krishnan SK, Singh E, Singh P, Meyyappan M, Nalwa HS (2019) A review on graphene-based nanocomposites for electrochemical and fluorescent biosensors. RSC Adv 9:8778–8881
17. Nag A, Mitra A, Mukhopadhyay SC (2018) Graphene and its sensor-based applications: a review. Sensor Actuat B-Phys 270: 177–194
18. Baig N, Saleh TA (2018) Electrodes modified with 3D graphene composites: a review on methods for preparation, properties and sensing applications. Microchim Acta 185:283
19. Idowu A, Boesl B, Agarwal A (2018) 3D graphene foam-reinforced polymer composites – a review. Carbon 135:52–71
20. Lu L (2018) Recent advances in synthesis of three-dimensional porous graphene and its applications in construction of electrochemical (bio)sensors for small biomolecules detection. Biosens Bioelectron 110:180–192
21. Baranwal A, Kumar A, Priyadharshini A, Oggu GS, Bhatnagar I, Srivastava A, Chandra P (2018) Chitosan: An undisputed biofabrication material for tissue engineering and bio-sensing applications. Int J Biol Macromol 110:110–123
22. Hu X, Goud KY, Kumar VS, Catanante G, Li Z, Zhu Z, Marty JL (2018) Disposable electrochemical aptasensor based on carbon nanotubes- V2O5-chitosan nanocomposite for detection of ciprofloxacin. Sensor Actuat B-Chem 268:278–286
23. Li Y, Liu Y, Kim E, Song Y, Tsao CY, Teng Z, Gao T, Mei L, Bentley WE, Payne GF, Wang Q (2018) Electrodeposition of a magnetic and redox-active chitosan film for capturing and sensing metabolic active bacteria. Carbohydr Polym 195:505–514
24. Wu Z, Guo F, Huang L, Wang L (2018) Electrochemical nonenzymatic sensor based on cetyltrimethylammonium bromide and chitosan functionalized carbon nanotube modified glassy carbon electrode for the determination of hydroxymethanesulfinate in the presence of sulfite in foods. Food Chem 259:213–218
25. George JM, Antony A, Mathew B (2018) Metal oxide nanoparticles in electrochemical sensing and biosensing: a review. Microchim Acta 185:358
26. Liu A, Kou W, Zhang H, Xu J, Zhu L, Kuang S, Huang K, Chen H, Jia Q (2020) Quantification of trace organophosphorus pesticides in environmental water via enrichment by magnetic-zirconia nanocomposites and online extractive electrospray ionization mass spectrometry. Anal Chem 92:4137–4145
27. Zhang QR, Bolisetty S, Cao YP, Handschin S, Adamcik J, Peng QM, Mezzenga R (2019) Selective and efficient removal of fluoride from water: in situ engineered amyloid fibril/ZrO2 hybrid membranes. Angew Chem Int Edit 58:6012–6016
28. Reddy CV, Reddy IN, Harish VVN, Reddy KR, Shetti NP, Shim J, Aminabhavi TM (2020) Efficient removal of toxic organic dyes and photoelectrochemical properties of iron-doped zirconia nanoparticles Chemosphere:239
29. Reddy CV, Reddy IN, Ravindranadh K, Reddy KR, Shetti NP, Kim D, Shim J, Aminabhavi TM (2020) Copper-doped ZrO2 nanoparticles as high-performance catalysts for efficient removal of toxic organic pollutants and stable solar water oxidation. J environ manage 260:
30. Reddy CV, Reddy IN, Reddy KR, Jaesool S, Yoo K (2019) Template-free synthesis of tetragonal co-doped ZrO2 nanoparticles for applications in electrochemical energy storage and water treatment. Electrochim Acta 317:416–426
31. Hou XD, Tang S, Guo XX, Wang LC, Liu X, Lu XF, Guo Y (2018) Preparation and application of guanidyl-functionalized graphene oxide-grafted silica for efficient extraction of acidic herbicides by box-Behnken design. J Chromatogr A 1571:65–75

32. Hou X, Liu S, Zhou P, Li J, Liu X, Wang L, Guo Y (2016) Polymeric ionic liquid modified graphene oxide-grafted silica for solid-phase extraction to analyze the excretion-dynamics of flavonoids in urine by box-Behnken statistical design. J Chromatogr A 1456:10–18
33. Zeng L, Zhang Y, Wang H, Guo L (2013) Electrochemical behavior of luteolin and its detection based on macroporous carbon modified glassy carbon electrode. Anal Methods 5:3365
34. Pang P, Liu Y, Zhang Y, Gao Y, Hu Q (2014) Electrochemical determination of luteolin in peanut hulls using graphene and hydroxyapatite nanocomposite modified electrode. Sensor Actuat B-Chem 194:397–403
35. Ma Y, Kong Y, Xu J, Deng Y, Lu M, Yu R, Yuan M, Li T, Wang J (2020) Carboxyl hydrogel particle film as a local pH buffer for voltammetric determination of luteolin and baicalein. Talanta 208: 120373
36. Tesio AY, Granero AM, Vettorazzi NR, Ferreyra NF, Rivas GA, Fernández H, Zon MA (2014) Development of an electrochemical sensor for the determination of the flavonoid luteolin in peanut hull samples. Microchem J 115:100–105

Publisher's Note Springer Nature remains neutral with regard to jurisdictional claims in published maps and institutional affiliations.